Constraints on the δ^2H diffusion rate in firn from field measurements at Summit, Greenland

L.G. van der Wel[1,*], H.A. Been[1], R.S.W. van de Wal[2], C.J.P.P. Smeets[2], and H.A.J. Meijer[1]

1 Centre for Isotope Research (CIO), Energy and Sustainability Research Institute Groningen (ESRIG), University of Groningen, NL-9747AG Groningen, the Netherlands
2 Institute for Marine and Atmospheric Research Utrecht (IMAU), University of Utrecht, NL-3584 CC Utrecht, the Netherlands
* present address: Institute of Climate and Environmental Physics, University of Bern, CH-3012 Bern, Switzerland

Correspondence e-mail: h.a.j.meijer@rug.nl

Abstract

We performed detailed ^{2}H isotope diffusion measurements in the upper 3 meters of firn at Summit, Greenland. Using a small snow gun, a thin snow layer was formed from ^{2}H-enriched water over a 6 x 6 m^2 area. We followed the diffusion process, quantified as the increase of the $\delta^{2}H$ diffusion length, over a four years period, by retrieving the layer once per year by drilling a firn core and slicing it into 1 cm layers and measuring the $\delta^{2}H$-signal of these layers.
We compared our experimental findings to calculations based on the model by Johnsen et al. (2000), and found substantial differences. The diffusion length in our experiments increased much less over the years than in the model. We discuss the possible causes for this discrepancy, and conclude that several aspects of the diffusion process in firn are still poorly constrained, in particular the tortuosity.

1 Introduction

The relative abundance of the stable isotopes ^{2}H and ^{18}O in ice cores is one of the most powerful proxies of the paleo-temperature over the last 800 kyrs (Jouzel and EPICA community, 2007). The global meteoric water cycle acts as a global scale isotope distillation system, through a continuous process of evaporation and condensation. It leads to a depletion of the abundance of heavier isotopes in the water molecules, which depletion increases with higher latitudes or rather, in fact, with lower temperature. In the polar regions, especially on Antarctica and Greenland, the precipitation containing this temperature-dependent isotope content is conserved, and by drilling deep ice cores on strategic places on these ice caps, the precipitation of over hundred thousand years (Dahl-Jensen et al., 2013; Johnsen et al., 2001) or even close to a million years (Oerter et al., 2004; Stenni et al., 2010) can be recovered. Accurate, high spatial resolution isotope abundance measurements on this ice core material then reveal the "proxy" temperature signal.
As said, the signals are proxies, implying that their relation with past temperature is solid, but not necessarily linear, and not even of a constant character through time or in space. Most of this "proxy" character is due to the complex and time-dependent relation between temperature and circulation patterns in the atmosphere, influencing the behaviour of the isotope distillation system. Some of it, however, is due to processes that influence the isotopic abundance pattern after deposition. Apart from processes acting only on very fresh snow still at or close to the surface (firn ventilation and sublimation, (Neumann and Waddington, 2004; Sokratov and Golubev, 2009)), the main process is diffusion. This smears out, and can eventually wash away, spatial gradients in the isotope abundances. Diffusion takes place in the solid ice phase, but especially, at a rate some 5 orders of magnitudes higher, in the firn phase. In the latter case, the diffusion process is governed by the continuous evaporation and condensation of ice particles into and from the air channels. While in the vapour phase, the water molecules travel a certain distance before freezing back to the solid phase. The process is relatively fast, especially in the first years after deposition, when the firn density is still low, and summer temperatures still affect the firn temperature. On the central Greenland ice sheet, the isotope diffusion process decreases the seasonal cycle amplitude by typically a factor of five, and effectively influences all time scales of decadal variability and shorter (Andersen et al., 2006a; Vinther et al., 2006).

Isotope diffusion in firn has been discovered by Langway (1967), and is well-understood in the qualitative sense. Quantification, however, is more difficult, as the rate depends critically on the density of the firn and, moreover, on the tortuosity of the firn, i.e. the shape and size of the air channels between the ice crystals. Furthermore even grain size might play a role. Several laboratory experiments have been performed on the isotope diffusion rate (Jean-Baptiste et al., 1998; Pohjola et al., 2007; van der Wel et al., 2011a), and expressions for the rates that include a parameterization for the tortuosity dependence have been formulated (Cuffey and Steig, 1998; Johnsen et al., 2000; Whillans and Grootes, 1985), and tested (Pohjola et al., 2007; van der Wel et al., 2011a).
Corrections for isotope diffusion (usually to reconstruct the original precipitation signal: "back-diffusion") are currently performed routinely. The last publication that we are aware of that shows the "raw", uncorrected isotope signals together with the corrected ones is by Johnsen (1977). So, in spite of the fact that the process is difficult to quantify, back-diffusion is applied routinely for the interpretation of ice cores, even for short(er) time scales (Bolzan and Pohjola, 2000; Vinther et al., 2006).
As the process is difficult to quantify, we found the isotope diffusion rate worth further investigation, especially since: (1) isotope diffusion has gained renewed attention, after the discovery (by Johnsen et al. (2000)) that the difference of the diffusion rate for ^{2}H and ^{18}O ("differential diffusion") is dependent only on the temperature of the firn. Differential diffusion has thus the potential of becoming a powerful new paleotemperature proxy by itself (Simonsen et al., 2011; van der Wel, 2012). (2) All laboratory experiments on diffusion rates have been performed on artificially produced "firn": shaved ice flakes (Jean-Baptiste et al., 1998; Pohjola et al., 2007), or, at best, snow produced by a snow gun (van der Wel et al., 2011a). However, it was realized that the tortuosity, the 3D-shape of the air channels between the crystals, is important for the diffusion rate, and it is well conceivable that this differs considerably between artificial "snow" and real snow. (3) Most laboratory experiments have concentrated on the high density regime, where tortuosity effects are most pronounced, but where the diffusion process is slow. Here, we concentrate on the initial phase of firnification where diffusion is fastest.
For these three reasons we decided to design and perform a field experiment in which we could measure the ^{2}H isotope diffusion rate for real snow. Using a snow gun, we produced a thin layer of artificially made snow, enriched in ^{2}H (enriched ^{18}O water is too expensive and rare for such a field experiment), on a field site at Summit station, Greenland, a site with temperatures below 0°C all year (at least prior to 2012). In the four years that followed, 2008-2011, we went back to the place four times and drilled shallow cores (from 1 to close to 4 meters over the years) in which we recovered our original layer, now diffused well into the original firn surrounding it. Isotope analysis in the laboratory yielded the width of the diffused profile over the years. Together with the temperature of the layer, which was logged, and the measured density, this enabled us to compare the actually measured diffusion rate with the value from the generally used expression and parameterization by Johnsen et al. (2000).
In the following chapters, we start with the theoretical description of isotope diffusion, including our approach to numerically simulate our experiments. Next, we describe the field experiment. After that, we present the results of our measurements, and discuss those extensively. We end with some conclusions and a design for a follow-up experiment.

2 Isotope Diffusion in firn

In general, diffusion is the macroscopic description of microscopic random movements that, in combination with a gradient in the concentration of a certain constituent, cause a decrease of this gradient. The most commonly used macroscopic description originates from Fick, a German 19th century physiologist. According to his second law, and considering only one spatial dimension the effects of diffusion on the isotope concentration C is described as:

$$\frac{\partial C}{\partial t} = \Omega \frac{\partial^2 C}{\partial z^2} \tag{1}$$

where Ω is the diffusion coefficient, also called diffusivity, and t and z are the temporal and spatial coordinates, respectively. In our specific case, C would be the concentration of water molecules containing a ^{2}H isotope. In practice, however, the ^{2}H-concentration is expressed as the deviation of this concentration from that of a reference material. This deviation is denoted by δ^2H and is defined as:

$$\delta^2\mathrm{H} = \frac{R_{\mathrm{sample}}}{R_{\mathrm{reference}}} - 1 \tag{2}$$

where R is the abundance ratio of the rare isotope with respect to the abundant isotope: ^{2}H/^{1}H. δ^2H is usually expressed in ‰. As the difference between concentration and ratio is very small for ^{2}H, to a good approximation the diffusion equation is also valid using δ^2H. Therefore, we may change (1) into:

$$\frac{\partial \delta^2\mathrm{H}}{\partial t} = \Omega_{f2} \frac{\partial^2 \left(\delta^2\mathrm{H}\right)}{\partial z^2} \tag{3}$$

where Ω_{f2} is the firn diffusivity for δ^2H, for which an expression was derived by Johnsen et al. (2000):

$$\Omega_{f2} = \frac{m p_{sat} \Omega_{a2}}{RT\tau\alpha_2}\left(\frac{1}{\rho_f} - \frac{1}{\rho_{ice}}\right) \tag{4}$$

Here m is the molar mass of water (in kg), R the gas constant (J/K) and T the temperature in Kelvin. ρ_f and ρ_{ice} are the firn and ice density (kg/m^3), respectively (ρ_{ice} = 917 kg/m^3). For the water vapour saturation pressure p_{sat} we use the parameterization given by Murphy and Koop (2005):

$$p_{sat} = e^{\left(9.550426 - \frac{5723.265}{T} + 3.53068\ln(T) - 0.00728332T\right)} \tag{5}$$

with p_{sat} in Pa and T in Kelvin. As p_{sat} is exponentially dependent on temperature, this parameter is the main cause for temperature dependence of the diffusion process. The other terms in (4), except the tortuosity τ (and m and R), are temperature-dependent as well: apart from the temperature itself, these are the ice-vapour fractionation factor α_2 and the diffusivity of deuterated water vapour in air Ω_{a2}. For the most abundant water molecule $^1H_2{}^{16}O$ the diffusivity in air is given in m^2 /s by Hall and Pruppacher (1976):

$$\Omega_a = 0.211 \cdot 10^{-4}\left(\frac{T}{T_0}\right)^{1.94}\left(\frac{p_0}{p}\right) \tag{6}$$

where T is the temperature, T_0 is 273.15 K, p is the pressure at Summit (680 hPa during summer, the time when the diffusion process is the most active) and p_0 equal to 1013 hPa (1 atmosphere).

For water molecules containing a ^2H atom, the diffusivity is slightly lower (Merlivat, 1978):

$$\Omega_{a2} = \frac{\Omega_a}{1.0251} \tag{7}$$

The ice vapour fractionation factors, that is the difference in ratio of rare and abundant isotopes in ice and vapour under equilibrium conditions, are functions of temperature and were measured by Merlivat and Nief (1967) for Deuterium:

$$\alpha_2 = 0.9098\, e^{\frac{16288}{T^2}} \tag{8}$$

Finally, the tortuosity τ depends on the structure of the open channels in the firn. We adopt – initially- the parameterization as a function of the density of the firn that was given by Johnsen et al. (2000):

$$\frac{1}{\tau} = 1 - 1.30\left(\frac{\rho_f}{\rho_{ice}}\right)^2 \text{ for } \rho_f \le 804.3\ \text{kg/m}^3 \tag{9}$$

This parameterization leads to increasingly high values for τ as the density ρ_f approaches the density of pore close-off. For lower densities, however, the effects due to tortuosity are assumed to be minor: according to this parameterization the value of τ varies between 1.15 and 1.25 in the density range of our experiment (300-350 kg/m^3). Of course, this paramterization is a gross oversimplification of the real process, as it neglects the influence of varying grain sizes and shapes. Nevertheless, it seems to have served its goal reasonably well under widely varying circumstances. Diffusion decreases gradients, and thus leads to an overall smoothing of the original signal. The general solution to the differential equation (3) given an initial profile $\delta H_0(z)$ is a convolution of this initial profile with a Gaussian distribution:

$$\delta^2\mathrm{H}(z,t) = \frac{1}{\sigma_2(t)\sqrt{2\pi}} \int_{-\infty}^{\infty} \delta^2\mathrm{H}_0(z') \exp\left(\frac{(z-z')^2}{2\sigma_2^2(t)}\right) dz' \tag{10}$$

The amount of smoothing, that is, how the values of the original profile δ^2H_0 at positions z' influence the value $\delta^2H(z,t)$, is determined by the width of the Gaussian curve σ_2. The physical meaning of this width is the diffusion length, which is the average displacement of the deuterated water molecules. In case the original distribution $\delta^2\mathrm{H}_0(z, t=0)$ is a Dirac distribution (infinite at z=0, and zero everywhere else, such that its total integrated area is M), equation (10) leads to:

$$\delta^2\mathrm{H}(z,t) = \frac{M}{\sigma_2(t)\sqrt{2\pi}} \exp\left(\frac{-z^2}{2\sigma_2^2(t)}\right) \tag{11}$$

The squared value of σ is directly related to the isotopic diffusivity in firn and the elapsed time:

$$\sigma_2^2(t) = \int_0^t 2\Omega_{f2}(t')\, dt' \tag{12}$$

In such an idealized case, the profile that would be recovered would show a pure Gaussian profile, and its width would be directly related to the diffusivity.
The calculation of the width of such a profile would simply require the numerical integration of equation (12). For each time step, Ω_{f2} needs to be calculated with the appropriate values for the variables (temperature and/or density) for that time step.

In reality, the original distribution $\delta^2\mathrm{H}(z,t=0)$ is of course never a Dirac function. In our experiment, however, the initial signal does resemble a Dirac function, but with a finite value for the peak value and a finite width of this peak. Furthermore, we deposit our layer of ^{2}H enriched snow on a background that is not constant, but shows the natural seasonal cycle (subject to diffusion during previous years). Finally, in our experiment we sample the firn layer with a limited spatial resolution (of 1 cm). Hence we use a numerical model for the simulation of our findings, taking these complications into account (see section 4.3).

Comparison of the numerically calculated σ's with those from the field experiment enable us to test the validity of equation (4), and the terms it contains (most notably the parameterization for the tortuosity, equation (9)). The isotope effects (equations (7) and (8)), and obviously the saturation pressure of water vapour (equation (5)) are generally considered to be well-known and are treated here as constants without uncertainty. Recently, Ellehoj et al. (2013) reinvestigated the ice-vapour fractionation factor α_2 (8) and found it to be larger, from ≈1% at -15°C to over 3% at -40°C. Although such changes are highly significant when studying, for example, the hydrological cycle, for our study such changes are of minor importance.

3 The field experiment

For the production of ^{2}H-enriched snow under polar field conditions, we built a snow gun installation. The snow gun itself was a small instrument designed for home garden use (CHS Snowmakers, type "Cornice"). The gun produces a very fine spray of droplets which precipitate as dry, fluffy snow, provided the ambient temperature is low enough (at most -5 °C, preferably several degrees lower). We built the necessary air compressor and water pump system on a compact, gasoline motor driven cart. The installation was capable of producing ≈ 300 kg of snow per hour. We produced snow on an area of typically 6 x 6 m^2, such that we would have ample space for drilling 2-3 hand cores per year for four years without interference. We aimed for a snow layer of 2-3 cm and allowed for loss of snow spraying outside the field, so we used about 1000 litres of water. We contained this amount of water in an inflatable children's paddling pool, which is easily transportable, and also forms a good thermal isolation (we added a foam mat underneath).

The water was enriched to a level of typically $\delta^2\mathrm{H}$ = 1000 ‰ by adding 250 g of pure D_2O (Sigma-Aldrich) (depending on the natural $\delta^2\mathrm{H}$-level of the water used).

In August 2007, we produced an area of ^{2}H-enriched snow in the field on pristine snow, about 2 km away from camp Summit (central Greenland, 72°35'N 38°25'W, elevation of 3216 m). The station is operated by the American-based CH2M HILL Polar Services (formerly Veco Polar Resources). In the summer months, there is frequent access for both people and equipment with Hercules C130 aircraft. Temperatures are always below 0°C (at least during the years of our field work).

On August 8, 2007, we produced our enriched layer in about 5 hours, using ≈ 1000 litres of local surface melt water, enriched to $\delta^2\mathrm{H}$ = 1294±3 ‰. We also dyed the water with a red food colorant, to make our produced snow layer visible. Figure 1 shows the site while producing snow. The wind speed was low that day, so most of the produced snow landed on our area (marked with poles). It was a sunny day, with temperatures reaching -5 °C, which impeded dry snow production. Therefore we produced snow at a reduced production rate. Still, the produced layer on parts of our area was ice rather than snow, especially close to the snow gun. After finishing the snow production, we

carefully inspected the area, such that we could try to avoid the places with ice formation when sampling in later years.

A thermistor was placed at the surface, co-located with our layer and connected to a data logger close to one of the poles. Temperatures were logged every 3 hours. In this way a high resolution continuous temperature record for our layer would be available.

Prior to our snow making, we took samples from the pristine snow layer for isotope analysis, to a depth of about 50 cm. We also performed snow density measurements, to the same depth, with 10 cm resolution.

The night after the snow was produced, the layer got covered under a few cm of fresh snow. Afterwards, the depth of the snow layer was monitored by the Summit crew members every month by measuring the height of each of the 5 poles that marked the field; this went on until the final sampling day in 2011. At that time our snow layer was close to 3 metres below surface.

These careful snow height measurements provided us with the information needed to recover our layer in the consecutive years. In the years 2008, 2009, 2010 and 2011 (that is 352, 643, 1102 and 1460 days after the production of the layer) we returned to Summit to drill shallow firn cores with a hand corer (Kovacs Mark II). We drilled 2-3 cores every year (labelled A, B, C), and made sure that we recovered the expected depth of our layer ± some 50 cm (as the depth registered at the five poles around our field scattered by 20-30 cm over the years). Figure 2 shows the depth of our layer as a function of time based on those pole height measurements, together with the points indicating the actual depth of the enriched layer (or rather the depth of the maximum δ^2H value) as revealed by the isotope measurements later in the lab.

Still in the field, we cut the cores into 1 cm slices with a custom built device, and stored the slices in individual air-tight plastic bags (Toppits Zipper). Soon after, we let the slices melt and pored them over into lockable plastic sample transport tubes (Elkay products) that had been tested for their long-term isotope integrity.

In the field, we also secured the logged temperatures of the past year, and in 2010 and 2011, we performed again 10 cm resolution density measurements, now also using our hand corer.

Back in our laboratory in Groningen, we performed δ^2H and $\delta^{18}O$ isotope ratio measurements on all samples using our routine equipment (van der Wel, 2012). The combined uncertainties were ±0.06 ‰ for $\delta^{18}O$ and 0.6 to 2‰ for δ^2H (depending on the level of enrichment). In all of the total of 10 cores drilled over the years, we found our enriched layer back, close to the depth expected based on the pole height measurements (see figure 2).

4 Results

4.1 Density and temperature

For the simulation of the diffusion of our enriched layer, reliable values for both the temperature and the density are the most important input values. Figure 3 shows the density measurements that we performed over the years, all measured close to the area of the enriched layer, grouped in a single plot. The depths have been shifted (using the information shown in figure 2) such that our enriched layer is at depth zero. The data show that our enriched layer, deposited in the end of summer is on top of a layer with lower density than the preceding and following winters. This summer-winter effect is beautifully demonstrated by Albert and Shultz (2002) from Summit in

2000, and our data are in agreement with their findings (shown in their figure 2). Based on their and our data we use an initial density of 300 kg/m^3 for our diffusion calculations, with a gradual increase of 10 (kg/m^3) /yr.

The temperature registration of the thermocouple, at the same depth as the layer, is shown in figure 4. Unfortunately, in spite of our efforts, two larger parts of the total temperature profile were lost. Figure 4 shows the interpolations that we made. We estimate the extra uncertainty in the diffusion calculations due to this omission to be minor. Fortunately, the first full year of data has been recovered. This is the part when the layer is still so shallow, that the diurnal temperature cycle (which we capture by our 3-hourly temperature sampling) is still noticeable (see insert in the figure for the first month). As the diffusion rate is exponentially dependent on temperature, capturing this first period in detail is crucial for the results of the numerical simulations.

4.2 Field diffusion profiles

For each sampling year, two-three records for both δ^2H and $\delta^{18}O$ were measured (labelled A to B,C). δ^2H contains the crucial diffusion information: the broadened (and weakened) profile around our original layer of enriched δ^2H. The quality of our collected profiles was variable. Some of the profiles showed one or two samples (= cm) that had δ^2H values almost as high as the original enriched water, whereas all other samples were close to the natural values. We attribute this to ice formation during the snow production, reducing diffusion rates dramatically. Fortunately, for every year we also had profiles without such irregularities, that showed a clear, Gaussian-shaped profile above background.

Figure 5 shows two of the δ^2H profiles, 2008B, and 2011A, respectively. The effect of diffusion is directly visible, both in the width of the peak, and in its height. For the quantitative determination of both, however, we need to correct for the natural δ^2H seasonal cycle that interferes with the diffused pattern of our original enriched layer. We used the $\delta^{18}O$ profile to reconstruct the natural δ^2H seasonal cycle. δ^2H and $\delta^{18}O$ in precipitation show both a very similar seasonal cycle, with the amplitude of the δ^2H cycle being around 8 times as large as that of $\delta^{18}O$. Contrary to that of δ^2H, the $\delta^{18}O$ seasonal cycle is not influenced by our layer: the water used was in fact recent snow at Summit, with $\delta^{18}O \approx -30$ ‰ very close to the value of the top layer of our field. In figure 5, $\delta^{18}O$ is shown as well, with scale ratio 1:8 with respect to the δ^2H scale. For the reconstruction of the natural δ^2H signal the δ^2H-$\delta^{18}O$ ratio for all our 10 profiles was fitted individually, by using the flanks of the profiles. Subsequently, we corrected our measurements for this reconstruction of the natural δ^2H signal, thereby obtaining the net diffusion profile.

For each of the four years, we had two profiles available (and even 3 for 2008 and 2010). Only one of these 10 profiles (2008A) was not useful: the deposited layer consisted only of ice and diffusion had hardly taken place. Figure 6 shows all other net δ^2H profiles, together with the Gaussian fits, after subtracting the background signal. The width of the fit, which is the diffusion length σ (see equations (10) and (11)), is also indicated.

Not all profiles are of equal quality: half of them showed the presence of ice inside our deposited layer, visible through one isolated high δ^2H value in the profile (on most occasions the ice layers had already been noticed in the field); as those points are not representative for the diffusion process, we discarded them. This happened for profiles 2008B, 2009B, 2010B, 2010C and 2011A. Furthermore, some points had to be discarded that resulted from contamination of samples with

snow/firn from other depths that happened during the coring process (such contamination was also visible in the $\delta^{18}O$ signal). Discarded points are shown in the plots in brown. Table 1 shows the results for the diffusion length σ and the net peak height for all profiles. The increase of σ as a function of time is clearly visible. Contrary to σ, the net peak height is not only dependent on the diffusion time, but also on the initial thickness of the enriched layer. Therefore the found peak height is expected to be variable within and between years.

The uncertainties given in the second column in table 1 are those from the fitting procedure. While they give a good indication for the fit quality, the final combined uncertainty in the results is, of course, considerably higher. The main experimental uncertainty lies in the representation of the "z-axis", the depth. We estimate this error to be ±3% of the value, leading to an error in σ of about 0.10. The icy character of our deposited layer in some profiles form another principal source of error: although on both sides of such an ice layer the firn diffusion process takes place, and we can thus use those profiles for a σ measurement, the width of the fitted Gauss-curve will still be influenced by the presence of the icy character of the original layer itself. Therefore, we have increased the uncertainties for such profiles to ±0.25 cm. The uncertainty caused by the $\delta^{18}O$-based background correction is negligible. The final attributed errors are given in the "uncertainty" column. Except for 2008, all measured values per year agree within these uncertainties. As each year had at least one core with, and at least one core without ice in our deposited layer, the fact that their diffusion lengths agree with each other shows that these ice layers did not influence the diffusion length significantly in this experiment.

4.3 Comparison with the numerical simulation

The simplest way of simulating our experiment is to numerically integrate equation (12) using the known temperature and density as a function of time (eq. 4). However, the real experimental situation is more complicated. To accurately simulate the experimental situation, we first calculated the diffused δ^2H pattern as a function of time from the original $\delta^2H(z, t = 0)$ pattern around our enriched layer with an added "pulse" of enriched δ^2H. We know the value of this enriched δ^2H (1294‰), but the thickness of the layer is unknown, and variable. Therefore we calculated the profiles for three initial layer thicknesses: 6, 18 and 30 mm. As the next step, we corrected the diffused pattern for the slight compaction that occurred (inversely proportional to the small increase in density) and we sampled the diffused patterns with the spatial resolution of the experiment (1 cm). Then, we simulated the correction for the natural δ^2H seasonal cycle using the also diffused and sampled $\delta^{18}O$ profile, in the same way as we did with the experimental profiles. Finally, we fitted the net δ^2H profile with a Gaussian function.

Figure 7 shows the results for σ achieved this way, as well as the σ from the direct integration of equation (12). The differences between the numerical calculations at variable initial thickness are quite small, especially for the values of σ for later years, indicating that the effects of sampling and the background correction are minimal. Figure 7 also contains the experimental diffusion lengths, and thereby embodies the main results of this work. Clearly, there is a systematic mismatch between the experimental results and the numerical simulations, increasing with time. To fit the data, the simulated curves need to be $\approx 25\%$ lower in the first year, up to $\approx 40\%$ in the final year. This implies a lowering of Ω_{f2} up to a factor of 2.5 (as σ is proportional to the square root of Ω_{f2}). This lowered fit curve is also shown in figure 7. (The black dotted line in between will be described

in the discussion section.) All in all, figure 7 suggests that there is either an experimental flaw, or one or more parameters included in equation (4), or equation (4) as a whole, are not adequate. Below we discuss various possibilities, influencing the average value of σ and its dependence on time.

The full numerical procedure also results in a peak height, which at any point of time is proportional to the width of the initial enriched δ^2H pulse. Indicated in figure 8 (red dots) are the actual peak height fits of the profiles (see table 1). They are compared to the numerical simulations for layers with initial thicknesses 6, 18 and 30 mm, for which the diffusion length is fitted to the experimental points in figure 7 (the red dotted line). All experimental points are in the range spanned by the numerical calculations. The values for the ice layers that we removed from our profiles are also indicated: the position of four out of five of them in this plot clearly corroborates them as ice layers, as an initial layer thickness of 30 mm is about the maximum realistic value for our snow layer.

5 Discussion

The considerable discrepancy between our experimental results and the numerical calculations based on Johnsen et al. (2000) came as a surprise. The theoretical description of the firn diffusion process by Johnsen et al. (2000), a further development of work by Johnsen (1977) and Whillans and Grootes (1985) has been used for the description (and back-correction) of diffusion in many ice core projects.

The large majority of the papers describes, or "back-corrects", the influence of firn diffusion as it is recorded in the ice below pore close-off. There, the ice carries the result of firn diffusion integrated over the entire firn phase. Examples of such work, restricted to Greenland, are Vinther et al. (2006), Masson-Delmotte et al. (2005), Andersen et al. (2006b), Jouzel et al. (1997),Vinther et al. (2010), White et al. (1997) and Simonsen et al. (2011). The latter publication concentrates on the so-called differential diffusion, the difference in diffusion between $\delta^{18}O$ and δ^2H, which is only dependent on the temperature of the firn while diffusion takes place. This idea was in fact the main subject of Johnsen et al. (2000).

Below we will dicuss three possible causes for the discrepancy. They are (1) our experimental conditions, especially the formed ice in the deposited layer, (2) a considerable influence of tortuosity already in the uppermost meters of the firn, contrary to the assumptions in Johnsen et al. (2000), and (3) invalidity of the assumption that no gradient in isotopic composition builds up within the firn grains.

5.1 Experimental conditions

The occurrence of an ice layer can practically block the diffusion process. We do, however, firmly believe that our results have not been seriously influenced by ice formation. Each year contained both a profile with, and one without the indication of ice formation inside our deposited layer. Yet, for each of the four years that we sampled the results for the diffusion length agree very well. As the occurrence of an ice layer almost stops the diffusion process (see e.g. van der Wel et al. (2011b)) one would expect large scattering within and between years if ice formation inside our deposited layer would indeed play an important role. The fact that they do not can be explained by

406 the fact that the water vapour from such an ice layer will immediately encounter natural snow layers
407 in which the diffusion process occurs naturally. Only the ice layer itself will continue to contain a
408 high level of enrichment and in the end produces a δ^2H value that needs to be excluded from the fit
409 to the data, as we did.
410 Even in the absence of ice, the density of our artificial snow layer is probably higher than that of
411 fresh Summit snow. When trying to fit the results of figure 7 using higher densities we find that we
412 would need a more or less plausible density of around 380 kg/m^3 for the first year, but increasingly
413 higher values for the subsequent years, up to 520 kg/m^3 for the 2011 results. Such compaction of a
414 layer, initially already denser than its surroundings, in just 4 years is unrealistic. Further more, again
415 the diffusion process will immediately encounter natural snow as soon as the process starts. So, in
416 the course of the years, with diffusion lengths getting larger and the signal profile getting dominated
417 by the region outside the original layer, one can expect any initial effect of higher density to
418 weaken. However, we observe the opposite: the deviation between our experimental results and the
419 simulations based on Johnsen et al. (2000) increases in the course of the years.
420
421 *5.2 Tortuosity*
422
423 The diffusion length σ is inversely proportional to the square root of the tortuosity τ. If the
424 discrepancy between our results and the numerical simulation would be entirely due to higher
425 tortuosity in our experiment than the range of 1.15-1.3 given by equation (9), we would need the
426 tortuosity to be between 2.5 and 3. To see to what extent this would be plausible, we have gathered
427 relevant information from literature both describing firn isotope diffusion, and gas diffusion. To
428 facilitate a proper comparison, we first have to define the tortuosity in an unambiguous manner:

429 $$\Omega_f = \frac{\Omega_a \phi}{\tau}, \text{ with the porosity } \phi = 1 - \frac{\rho_f}{\rho_{ice}} \quad (13)$$

430 Here Ω_a is the diffusivity of the compound (water vapour in our case, or more precisely deuterated
431 water vapour) through a certain area of free air, and Ω_f the effective diffusivity through that same
432 area, but now filled with firn. The porosity ϕ accounts for the effective open area available for the
433 diffusion process, whereas the tortuosity accounts for the shape of the air channels. In the case of
434 perfectly straight air channels, τ would be 1.
435 The Whillans and Grootes model (Whillans and Grootes, (1985)) was the first to describe firn
436 diffusion in a detailed manner, but they did not include the influence of tortuosity. Instead of the
437 porosity, they included the density at pore close-off ρ_c:

438 $$\phi^* = 1 - \frac{\rho_f}{\rho_c} \quad (14)$$

439 Using this ϕ^* is equivalent to using equation (13), with

440 $$\tau = \frac{\phi}{\phi^*} = \frac{1 - \rho_f / \rho_{ice}}{1 - \rho_f / \rho_c} \quad (15)$$

441 As the difference between ρ_{ice} and ρ_c is rather small (Whillans and Grootes (1985) used 830 kg/m^3
442 for ρ_c), effective tortuosity values remain close to 1 except for densities approaching ρ_c.
443 Cuffey and Steig, (1998) performed a detailed, that is time-resolved studies of firn diffusion
444 showing the dampening of the seasonal cycle in $\delta^{18}O$ in the shallow GISP-B core (based on the data
445 published by Stuiver and Grootes, (2000) and Stuiver et al. (1995)), and compared that to the

Whillans and Grootes (1985) model (taking the low atmospheric pressure at Summit into account). They concluded that the model agreed well for the upper meters (starting, however, from a depth of 1.5 meter), but that the diffusion effects produced by the model were too large for larger depths. The diffusivity of the model needed to be decreased by a factor of about 1.7 to match the data. They built this into the model by decreasing the maximum density at which firn diffusion still occurs, from 830 down to (a fitted best value of) 730 kg/m^3. Using equation 15 their results can again be expressed as using a tortuosity factor that is now considerably higher than in the original Whillans and Grootes (1985) model. However, even in this study the depth resolution is limited to the length of one seasonal cycle (typically 50 cm), they ignored the top 1.5 meters, and their numerical procedure concentrated on the amplitude of the seasonal cycle only, not taking into account for example the diffusion differences between original summer and winter snow. The temperature driving the diffusion process is parameterized.

Johnsen et al. (2000) modified the Whillans and Grootes (1985) model, the main difference being the explicit introduction of the tortuosity factor. Other differences, with relatively small (<5%) influence, are a different parameterization of the water vapour diffusivity through free air, and the more complete treatment of the isotope effects. The tortuosity that Johnsen et al. (2000) used (equation 9) is based on a fit to gas diffusion measurements by Schwander et al., (1988), performed on firn samples from Siple station, Antarctica. The density range of these measurements was between 500 and 750 kg/m^3. Schwander et al. (1988) present the tortuosity as it is defined in equation (13) in their figure 5. Tortuosity values they found increased with the density from 2 to 7. They also provided a table (their table 1) that may give rise to some confusion. The effective diffusivity that is given there is in fact Ω_f / ϕ ("the flux per unit cross section in the open pores") (J. Schwander, pers comm, 2014). So, dividing the diffusivity given in that table by the open air diffusivity Ω_a directly yields $1/\tau$.

Their results for tortuosity were generally, although coarsely, confirmed by Jean-Baptiste et al. (1998), who did the first diffusion measurements on deuterium isotopes in firn: they measured the isotope diffusion around the connection of firns with distinctly different isotopic composition. The firn was, in fact, crushed ice. They used densities between 580 and 760 kg/m^3. Both the Schwander et al. (1988) results, and those by Jean-Baptiste et al. (1998) have thus been performed for higher densities only. Using the Schwander et al. (1988) parameterization by Johnsen et al. (2000) for our experiment, with densities varying from 300 to 350 kg/m^3, means a substantial extrapolation.

More recent measurements of firn diffusivity are presented in studies by Pohjola et al. (2007), and by van der Wel et al. (2011a). Both studies have improved on the work by Jean-Baptiste et al. (1998), since they have identified the interface between the two stacks with different isotopic composition as the weak spot of such experiments. By connecting several layers of different thickness they could identify possible problems with these interfaces, for example when such an interface was much more porous than the bulk material. Due to these effects, the results by Pohjola et al. (2007), at a density range of 480-500 kg/m3, did not produce consistent results for the tortuosity. Van der Wel et al. (2011a), however, managed to make an ideal multi-layer snow stack (produced with the same snow gun that we used in the present study). At a density of 415 kg/m^3, they were able to fit their diffused isotope profiles using the expression by Johnsen et al. (2000), thereby finding a tortuosity of 1.18±0.08 (compared to the value 1.36 that follows from equation 9). Whereas this latter information indicates tortuosity values hardly above 1 for low densities, various gas diffusion measurements show considerably higher values. Fabre et al. (2000) performed gas diffusivity measurements on site in Vostok, Antarctica, and on an alpine site (Col du Dome). They

express their results in the same fashion as Schwander et al. (1988)(they also show their results for comparison), and also give various model results for the tortuosity. Albert and Shultz, (2002) performed detailed gas diffusivity and permeability measurements on the top 10 meters of snow and firn on Summit station. They mention the tortuosity, defined in their paper as the reciprocal from our equation (13) as a side result, and quote the value of ~ 0.5 for the top layer of the snow. Looking at their data, however, it seems that they used a different definition for the tortuosity, and actually determined the ratio Ω_f/Ω_a to be 0.5. In more recent work by the same group, they avoid the term tortuosity altogether, and instead report on the Ω_f/Ω_a ratio.

Adolph and Albert, (2013) describe an improved way to measure gas diffusivity through firn, and they report a series of diffusion measurements performed on firn from Summit. From the results in their table 1 (in which they also quote their previous result from 2002) we can deduce the tortuosity as defined in equation (13). A next paper by the same authors (Adolph and Albert, 2014) reports on even more diffusivity measurements (and includes the ones reported in 2013).

Recently several large firn gas transport studies were published, one of them (Buizert et al., 2012) concentrating on the NEEM site on Northern Greenland. These authors tuned six firn air transport models to firn concentration measurements of a set of ten reference trace gases. Whereas the fit quality of the tracer concentrations is high, for the upper 4,5 meters the fit is underdetermined, and the spread of the molecular diffusivity profiles for CO_2 is large. Furthermore, convective mixing plays a role in modelling these upper 4,5 meters, a process that influences gas transport far more than the firn itself (see below). In direct firn gas diffusion experiments convective mixing is avoided, making such results more useful for describing firn diffusivity.

We give an overview of the tortuosity from all these results, according to our equation (13), in figure 9. This figure includes the tortuosity by Cuffey and Steig (1998) that follows from eq (15), and the parameterization for the Schwander et al. (1988) data used by Johnsen et al. (2000) (and thus also by us in the previous chapters). Furthermore, as a lower limit, we have included the theoretical result by Weissberg (1963), which he derived for spheres that can partly overlap or even fuse:

$$\frac{\Omega_f}{\Omega_a} = \frac{\phi}{1 - \frac{1}{2}\ln(\phi)} \tag{16}$$

Using equation (13) this is equivalent to

$$\tau = 1 - \tfrac{1}{2}\ln(\phi) \tag{17}$$

Looking at figure 9, we observe large scatter indeed. In the higher density region the tendency towards higher values for τ is clear, but there is a considerable discrepancy between the Schwander et al. (1988) values (based on CO_2 and O_2 diffusion through firn from Siple Dome, Antarctica) and the Fabre et al. (2000) ones (Vostok, Antarctica and the Col du Dome alpine site based on SF_6 and CO_2 diffusion) on the one hand, and the results by Adolph and Albert (2014) (using SF_6 diffusion through firn from Summit station) on the other. Although the Adolph and Albert (2014) results show some higher values, in general their results for τ are much lower[1], and thus the diffusion process would occur more rapidly. The real firn vapour diffusivity experiments by Jean-Baptiste et al. (1998), especially the highest density measurement, seems to corroborate the Schwander et al. (1988) and Fabre et al. (2000) results. Furthermore, as is clear from the work of

[1] Figure 6 in (Adolph and Albert, 2013) suggests the opposite. This is, however, because the authors interpreted the results in table 1 of Schwander et al. (1988) as Ω_f, whereas they are in fact Ω_f/ϕ (Adolph, and Schwander, 2014, pers. comm.)

Cuffey and Steig (1998), the total firn diffusion process on Summit can be described using their parameterization, which is not very different from the Schwander et al. (1988) measurements, and the Johnsen et al. (2000) parameterization.

However, the Adolph and Albert (2014) results also suggest higher values for τ at lower densities. This is in contrast with the only firn vapour measurement at low densities by van der Wel et al. (2011a), that gives a value that is lower than the Weissberg (1963) theoretical model. In contrast to that, the Adolph and Albert (2014) results suggest that a higher tortuosity in the low density region, of ≈ 1.5 is probably a better choice than the low values given by the extrapolation of the Johnsen et al. (2000) parametrization. The value range of 2.5-3, however, that we need to fit our data, is not supported by any data in the low density range. In figure 7, we show the numerical results for σ using a fixed tortuosity of 1.6. Whereas for the first year agreement is reasonable, in the following years the deviation increases: in the experiments, diffusion is slowing down, and this is unlikely to be caused by tortuosity (or density) increases.

The clearest conclusion of all, however, is that the parameterization of τ as a function of density (or porosity) is an oversimplification. Albert and Shultz (2002) show the structural changes of the fresh snow in its first years: whereas the density hardly changes, grain size rapidly grows, and the permeability (and likely also the diffusivity) increases. In that paper, they report a single diffusivity result (included in figure 9) on the top 20 cm of the firn, yielding $\tau = 1.36$ for ρ=326 kg/m^3. This suggests that for the youngest firn, time since deposit is a more important parameter than density. Furthermore, τ will have a different course in time for winter than for summer snow.

All in all, we conclude that for the simulation of our experiment, choosing a τ of ≈ 1.6 would be a fair choice given the data available, but a value range of $\tau = 2.5$-3, needed to fit our data using the Johnsen et al. (2000) simulation, is not plausible.

5.3 Isotope homogeneity within the firn grains

In the model by Johnsen et al. (2000), several assumptions have been made: -the effects of firn ventilation are negligible, -there is continuous isotopic equilibrium between the ice grain surfaces and the vapour, and -the ice grains themselves remain isotopically homogeneous. One or more of these issues have been addressed by several authors, among which Whillans and Grootes (1985), Jean-Baptiste et al. (1998), Johnsen et al. (2000) themselves and Neumann and Waddington (2004). The latter paper describes a very detailed, numerical model in which in the first place the influence of firn ventilation is quantified. They conclude that isotope exchange in the upper few meters is more rapid than follows from models such as that of Whillans and Grootes (1985) and Johnsen et al. (2000). However, they also state that the ventilation process is especially important in low accumulation zones, such as the Antarctic plateau. For the Summit site, its influence will probably only be marginal. Moreover, whereas firn ventilation might lead to changes in the overall isotopic composition, its character will not be the same as diffusion; especially it will not influence the diffusion pattern, and thus the diffusion length fit, of our enriched layer.

The model by Neumann and Waddington (2004) also allows for a disequilibrium between the ice grain surface and the vapour. Although the isotope exchange rate is not well-known, they conclude that the ice phase is not in isotopic equilibrium with the vapour at any depth in the firn. This effect would slow down the influence of diffusion. Somewhat surprising however, these authors assume the grains themselves to be and remain isotopically homogenous. This is in fact the point that the other authors touch upon. Isotope diffusion in ice, and thus inside the grains, is 10 orders of

magnitude smaller than vapour diffusion through air. At -20°C, for example, the solid ice diffusivity is about 1×10^{-15} m^2/s (Whillans and Grootes (1985)), whereas vapour diffusion through air, according to equation 6 (Hall and Pruppacher, 1976), yields 2.7×10^{-5} m^2/s at Summit. In contrast, the water molecules spend 5 to 6 orders of magnitude more time in the solid than in the vapour phase (depending both on temperature and density of the firn). Both Whillans and Grootes (1985) and Johnsen et al. (2000) have incorporated this into their model by dividing the free vapour diffusion rate by this residence time ratio. Nevertheless, the solid ice diffusivity remains some 5 orders of magnitude slower than the effective vapour diffusion. Whillans and Grootes (1985) have investigated this and concluded that, given the average size of the firn grains, the isotopic homogeneity assumption is valid. Jean-Baptiste et al. (1998), however, show in a numerical model that their model description of their firn diffusion experiment would indeed be influenced for grain sizes of 1mm and larger. Johnsen et al. (2000) conclude that grain homogeneity will not occur based on ice diffusion alone "for the coarse grained (2 mm) summer layers". As they on the other hand conclude from observations that the isotopic seasonal cycle can disappear completely due to diffusion, they propose grain boundary migration as a different mechanism for more rapid grain isotope homogenization.

The ratio between the effective firn vapour diffusion and solid ice diffusion is the largest for low densities, as then the solid to vapour residence time ratio is the lowest. These are the circumstances of our experiment. Furthermore, the detailed microstructure experiments by Albert and Shultz (2002) show substantial growth of grain size in the first years after deposition. Together, these circumstances will probably cause a substantial inhomogeneity in the ice grains, thereby slowing down diffusion to below the rate described by equation (4).

6 Conclusions and outlook

With this experiment, we have observed isotope diffusion in the natural setting of Summit in the first four years after deposit down to about 3 meters depth. The idea of determining the diffusion length as the Gaussian width of an initial thin layer substantially enriched in deuterated water worked very well indeed. The results, however, indicate a substantially lower diffusivity than expected based on the well-established model by Johnsen et al. (2000). Our attempt to explain this difference brought us to the following conclusions:

- -Although we can not be fully sure whether the characteristics of the enriched layer itself, with some local ice formation, has slowed down the diffusivity, it is very likely that the diffusion lengths we have obtained resemble the true diffusivity of deuterated water in the upper layers of Summit firn, because the diffusion takes place in the original snow layers after some time.
- Tortuosity is in general poorly characterised. Several of the firn and gas diffusion experiments over the years lead to a very scattered total picture. The parametrization used by Johnsen et al. (2000) is probably not correct for Summit; based on recent gas diffusion experiments by Adolph and Albert (2014), tortuosity is probably considerably larger in the uppermost layers, but in contrast not as large in the deeper firn. Density is a poor measure for tortuosity, certainly in the upper meters of firn, and considerable differences between summer and winter layers are likely to exist.

- Nevertheless, the discrepancy between our results and the Johnsen et al. (2000) model cannot be explained by higher tortuosity alone, as the value that would be needed to fit our data is definitely outside the plausible range.
- It is likely that isotopic inhomogeneity exists within the ice grains in the firn, as the vapour diffusion process is orders of magnitude faster than solid ice diffusion. This effect is only partly compensated by the much longer residence time of the molecules in the solid phase. This inhomogeneity, and its slowing effect on diffusion, depends critically on grain size. In the first years after snow deposition, grains tend to grow (Albert and Shultz, 2002), thereby effectively slowing down diffusion. Of the three possible causes for the discrepancy between our data and the simulations, isotopic inhomogeneity is thus the most plausible: it would explain why gas diffusion measurements (and thus also the parameterization used by Johnsen et al. (2000)) are not entirely valid for firn vapour diffusion. In the first stage of the diffusion process, the part that our experiment monitors, ice grain inhomogeneity would slow down the diffusion process, but in a later stage the inhomogeneity would diminish or even disappear again. Combined with lower values for the tortuosity at greater density (such as for instance those by Adolph and Albert (2014)) the total, integrated diffusivity would still fit to the well-known isotope signals in the ice. To prove (or disprove) this hypothesis, a new model framework needs to be developed to incorporate grain inhomogeneity into the model. Jean-Baptiste et al. (1998) and especially Neumann and Waddington (2004) have shown pathways towards such models.
- Although the model by Johnsen et al. (2000) has been used extensively and successfully, this has to our knowledge never been done in the amount of detail we present. Rather, it has been used to describe the integrated diffusion over the entire firn phase, expressed as the total diffusion length caused by it. This integrated diffusion length is a rather forgiving parameter: it does not matter whether the diffusion length grows rapidly initially and then slows down, or if it increases more steadily over the years. Moreover, due to compaction the diffusion length even decreases again, although the diffusion effects (such as the decrease of the amplitude of the seasonal cycle) of course are not lessened. According to the model, the major part of the diffusion length is built up in just the upper 10 meters (see also Simonsen et al. (2011)), and the maximum values are achieved around 30 meters depth; from then onwards, the compaction leads to a gradual decrease in diffusion length. These features of the model have, to the best of our knowledge, never been checked experimentally.

An experiment to perform such a decisive test would consist of two parts: first is the high resolution (typically 2 cm) isotope measurement of the upper ≈ 30 meters of a firn core. With a modern, laser-based isotope measurement system on-site, this would be probably feasible in just one summer season. If designed carefully, this set-up delivers the density of the firn as well. Second is reconstruction of the input function: the temperature, the precipitation events, and –ideally- their isotopic composition. In this way, the "virtual ice core" approach (van der Wel et al., 2011b) can be followed to reconstruct the non-diffused firn profile, and by comparing that profile to the data, diffusivity can be calculated with high temporal/spatial resolution. The results can then be compared to the output of the Johnsen et al. (2000) model, and to a model containing both the firn diffusion and the diffusion inside the grains. A valuable additional measurement would be isotope measurements on vapour in firn air at various depths. In this way the isotopic (dis)equilibrium could directly be assessed.

Summit would be the ideal spot for such an experiment: it has been in operation since 1988, and surface temperature and precipitation amounts have been logged since then. Furthermore, many scientific experiments run at Summit each year, many of them including stable isotope measurements.

Such a detailed study would finally enable us to describe isotope diffusion in firn in a reliable, quantitative way. The results of such a study would especially be crucial for the use of differential diffusion to reconstruct paleo-temperatures: the way the diffusion process behaves through the firn layer determines the weighted average of the temperature that is conserved in the differential diffusion signal. If the upper few meter diffusion is less prominent than the Johnsen et al. (2000) model suggests, this weighted average would be far less sensitive to the high summer day temperatures than is assumed at present.

Acknowledgements

A substantial part of this project has been funded by the polar programme of the Netherlands Organisation for Scientific Research (NWO) with project numbers 851.30.015, 851.30.22, and 851.20.038-B, for which support we are grateful.

Staff and crew from CH2MHill Polar Services at Summit and Kangerlussuaq are thanked for their enthusiastic and skilful assistance over the years. The NSF is thanked for granting us access to the fantastic Summit infrastructure.

Thanks to Henk Snellen and Ellen den Ouden for their assistance in the field. Laboratory technicians Berthe Verstappen, Janette Spriensma and Henk Jansen are acknowledged for the isotope analyses, and Jenny Schaar for assisting with the numerical code.

References

Adolph, A. and Albert, M. R.: An improved technique to measure firn diffusivity, Int J Heat Mass Tran, 61, 598–604, doi:10.1016/j.ijheatmasstransfer.2013.02.029, 2013.

Adolph, A. C. and Albert, M. R.: Gas diffusivity and permeability through the firn column at Summit, Greenland: measurements and comparison to microstructural properties, The Cryosphere, 8(1), 319–328, doi:10.5194/tc-8-319-2014, 2014.

Albert, M. R. and Shultz, E. F.: Snow and firn properties and air-snow transport processes at Summit, Greenland, Atm Env, 36(15-16), 2789–2797, doi:10.1016/S1352-2310(02)00119-X, 2002.

Andersen, K. K., Ditlevsen, P. D., Rasmussen, S. O., Clausen, H. B., Vinther, B. M., Johnsen, S. J. and Steffensen, J. P.: Retrieving a common accumulation record from Greenland ice cores for the past 1800 years, J Geophys Res-Atmos, 111, D15106, doi:10.1029/2005JD006765, 2006a.

Andersen, K. K., Svensson, A., Johnsen, S. J., Rasmussen, S. O., Bigler, M., Rothlisberger, R., Ruth, U., Siggaard-Andersen, M.-L., Steffensen, J. P., Dahl-Jensen, D., Vinther, B. M. and Clausen, H. B.: The Greenland Ice Core Chronology 2005, 15-42 ka. Part 1: constructing the time scale,

708 Quaternary Sci Rev, 25(23-24), 3246–3257, doi:10.1016/j.quascirev.2006.08.002, 2006b.

709 Bolzan, J. F. and Pohjola, V. A.: Reconstruction of the undiffused seasonal oxygen isotope signal in
710 central Greenland ice cores, J Geophys Res-Oceans, 105(C9), 22095–22106,
711 doi:10.1029/2000JC000258, 2000.

712 Buizert, C., Martinerie, P., Petrenko, V. V., Severinghaus, J. P., Trudinger, C. M., Witrant, E.,
713 Rosen, J. L., Orsi, A. J., Rubino, M., Etheridge, D. M., Steele, L. P., Hogan, C., Laube, J. C.,
714 Sturges, W. T., Levchenko, V. A., Smith, A. M., Levin, I., Conway, T. J., Dlugokencky, E. J.,
715 Lang, P. M., Kawamura, K., Jenk, T. M., White, J. W. C., Sowers, T., Schwander, J. and Blunier,
716 T.: Gas transport in firn: multiple-tracer characterisation and model intercomparison for NEEM,
717 Northern Greenland, Atmos Chem Phys, 12(9), 4259–4277, doi:10.5194/acp-12-4259-2012, 2012.

718 Cuffey, K. M. and Steig, E. J.: Isotopic diffusion in polar firn: implications for interpretation of
719 seasonal climate parameters in ice-core records, with emphasis on central Greenland, J Glaciol,
720 44(147), 273–284, 1998.

721 Dahl-Jensen, D., Albert, M. R., Aldahan, A., Azuma, N., Balslev-Clausen, D., Baumgartner, M.,
722 Berggren, A. M., Bigler, M., Binder, T., Blunier, T., Bourgeois, J. C., Brook, E. J., Buchardt, S. L.,
723 Buizert, C., Capron, E., Chappellaz, J., Chung, J., Clausen, H. B., Cvijanovic, I., Davies, S. M.,
724 Ditlevsen, P., Eicher, O., Fischer, H., Fisher, D. A., Fleet, L. G., Gfeller, G., Gkinis, V., Gogineni,
725 S., Goto-Azuma, K., Grinsted, A., Gudlaugsdottir, H., Guillevic, M., Hansen, S. B., Hansson, M.,
726 Hirabayashi, M., Hong, S., Hur, S. D., Huybrechts, P., Hvidberg, C. S., Iizuka, Y., Jenk, T.,
727 Johnsen, S. J., Jones, T. R., Jouzel, J., Karlsson, N. B., Kawamura, K., Keegan, K., Kettner, E.,
728 Kipfstuhl, S., Kjaer, H. A., Koutnik, M., Kuramoto, T., Koehler, P., Laepple, T., Landais, A.,
729 Langen, P. L., Larsen, L. B., Leuenberger, D., Leuenberger, M., Leuschen, C., Li, J., Lipenkov, V.,
730 Martinerie, P., Maselli, O. J., Masson-Delmotte, V., McConnell, J. R., Miller, H., Mini, O.,
731 Miyamoto, A., Montagnat-Rentier, M., Mulvaney, R., Muscheler, R., Orsi, A. J., Paden, J., Panton,
732 C., Pattyn, F., Petit, J. R., Pol, K., Popp, T., Possnert, G., Prie, F., Prokopiou, M., Quiquet, A.,
733 Rasmussen, S. O., Raynaud, D., Ren, J., Reutenauer, C., Ritz, C., Rockmann, T., Rosen, J. L.,
734 Rubino, M., Rybak, O., Samyn, D., Sapart, C. J., Schilt, A., Schmidt, A. M. Z., Schwander, J.,
735 Schuepbach, S., Seierstad, I., J P Severinghaus, S Sheldon, S B Simonsen, J Sjolte, A M Solgaard,
736 T Sowers, P Sperlich, H C Steen-Larsen, K Steffen, J P Steffensen, D Steinhage, T F Stocker, C
737 Stowasser, A S Sturevik, W T Sturges, A Sveinbjornsdottir, A Svensson, J L Tison, J Uetake, P
738 Vallelonga, Roderik S W Van de Wal, G van der Wel, B H Vaughn, B Vinther, E Waddington, A
739 Wegner, I Weikusat, J W C White, F Wilhelms, M Winstrup, E Witrant, E W Wolff, C Xiao, J
740 Zheng, and NEEM Community: Eemian interglacial reconstructed from a Greenland folded ice
741 core, Nature, 493(7433), 489–494, doi:10.1038/nature11789, 2013.

742 Ellehoj, M. D., Steen-Larsen, H. C., Johnsen, S. J. and Madsen, M. B.: Ice-vapor equilibrium
743 fractionation factor of hydrogen and oxygen isotopes: Experimental investigations and implications
744 for stable water isotope studies, Rapid Commun Mass Sp, 27(19), 2149–2158,
745 doi:10.1002/rcm.6668, 2013.

746 Fabre, A., Barnola, J.-M., Arnaud, L. and Chappellaz, J.: Determination of gas diffusivity in polar
747 firn: Comparison between experimental measurements and inverse modeling, Geophys Res Lett,
748 27(4), 557–560, doi:10.1029/1999GL010780, 2000.

749 Hall, W. D. and Pruppacher, H. R.: The Survival of Ice Particles Falling from Cirrus Clouds in
750 Subsaturated Air, J. Atmos. Sci., 33(10), 1995–2006, doi:doi: 10.1175/1520-
751 0469(1976)033<1995:TSOIPF>2.0.CO;2, 1976.

752 Jean-Baptiste, P., Jouzel, J., Stievenard, M. and Ciais, P.: Experimental determination of the

753 diffusion rate of deuterated water vapor in ice and application to the stable isotopes smoothing of
754 ice cores, Earth Planet Sc Lett, 158(1-2), 81–90, doi:10.1016/S0012-821X(98)00045-4, 1998.

755 Johnsen, S. J.: Stable isotope homogenization of polar firn and ice, IAHS red books series, 118,
756 210–219, 1977.

757 Johnsen, S. J., Dahl-Jensen, D., Gundestrup, N., Steffensen, J. P., Clausen, H. B., Miller, H.,
758 Masson-Delmotte, V., Sveinbjornsdottir, A. E. and White, J.: Oxygen isotope and
759 palaeotemperature records from six Greenland ice-core stations: Camp Century, Dye-3, GRIP,
760 GISP2, Renland and NorthGRIP, J Quaternary Sci, 16(4), 299–307, doi:10.1002/jqs.622, 2001.

761 Johnsen, S.J., Clausen, K., Cuffey, K., Hoffmann, K., Schwander, J. and Creyts, T.: Diffusion of
762 stable isotopes in polar firn and ice: The isotope effect in firn diffusion, edited by S. Johnsen, K.
763 Clausen, K. Cuffey, K. Hoffmann, J. Schwander, and T. Creyts, Physics of ice core Records (T.
764 Hondoh, editor) Hokkaido University Press, Sapporo, 2000.

765 Jouzel, J. and EPICA community, T.: Orbital and millennial Antarctic climate variability over the
766 past 800,000 years, Science, 317(5839), 793–796, doi:10.1126/science.1141038, 2007.

767 Jouzel, J., Alley, R. B., Cuffey, K. M., Dansgaard, W., Grootes, P., Hoffmann, G., Johnsen, S. J.,
768 Koster, R. D., Peel, D., Shuman, C. A., Stievenard, M., Stuiver, M. and White, J.: Validity of the
769 temperature reconstruction from water isotopes in ice cores, J Geophys Res-Oceans, 102(C12),
770 26471–26487, doi:10.1029/97JC01283, 1997.

771 Langway, C. C. J.: Stratigraphic analysis of a deep ice core from Greenland, Cold Regions
772 Research Engineering Laboratory Research Report, Hanover, NH, USA, 77, 1967.

773 Masson-Delmotte, V., Landais, A., Stievenard, M., Cattani, O., Falourd, S., Jouzel, J., Johnsen, S.
774 J., Jensen, D. D., Sveinsbjornsdottir, A., White, J. M. W., Popp, T. and Fischer, H.: Holocene
775 climatic changes in Greenland: Different deuterium excess signals at Greenland Ice Core Project
776 (GRIP) and NorthGRIP, J Geophys Res-Atmos, 110, D14102, doi:10.1029/2004JD005575, 2005.

777 Merlivat, L.: Molecular Diffusivities of $H_2{}^{16}O$, $HD^{16}O$, and $H_2{}^{18}O$ in Gases, J Chem Phys, 69(6),
778 2864–2871, doi:10.1063/1.436884, 1978.

779 Merlivat, L. and Nief, G.: Fractionnement Isotopique Lors Des Changements Detat Solide-Vapeur
780 Et Liquide-Vapeur De Leau A Des Temperatures Inferieures A 0 Degrees C, Tellus, 19(1), 122–
781 127, 1967.

782 Murphy, D. M. and Koop, T.: Review of the vapour pressures of ice and supercooled water for
783 atmospheric applications, Q J Roy Meteor Soc, 131(608, B), 1539–1565, doi:10.1256/qj.04.94,
784 2005.

785 Neumann, T. A. and Waddington, E. D.: Effects of firn ventilation on isotopic exchange, J Glaciol,
786 50(169), 183–194, doi:10.3189/172756504781830150, 2004.

787 Oerter, H., Graf, W., Meyer, H. and Wilhelms, F.: The EPICA ice core from Dronning Maud Land:
788 first results from stable-isotope measurements, Ann. Glaciol., 39, 307–312, 2004.

789 Pohjola, V. A., Meijer, H. A. J. and Sjoberg, A.: Controlled experiments on the diffusion rate of
790 stable isotopes of water in artificial firn, J Glaciol, 53(183), 537–546,
791 doi:10.3189/002214307784409379, 2007.

792 Schwander, J., Stauffer, B. and Sigg, A.: Air mixing in firn and the age of the air at pore close-off,

793 edited by H. Oeschger, Ann Glaciol, 10, 141–145, 1988.

794 Simonsen, S. B., Johnsen, S. J., Popp, T. J., Vinther, B. M., Gkinis, V. and Steen-Larsen, H. C.:
795 Past surface temperatures at the NorthGRIP drill site from the difference in firn diffusion of water
796 isotopes, Clim Past, 7(4), 1327–1335, doi:10.5194/cp-7-1327-2011, 2011.

797 Sokratov, S. A. and Golubev, V. N.: Snow isotopic content change by sublimation, J Glaciol,
798 55(193), 823–828, doi:10.3189/002214309790152456, 2009.

799 Stenni, B., Masson-Delmotte, V., Selmo, E., Oerter, H., Meyer, H., Roethlisberger, R., Jouzel, J.,
800 Cattani, O., Falourd, S., Fischer, H., Hoffmann, G., Iacumin, P., Johnsen, S. J., Minster, B. and
801 Udisti, R.: The deuterium excess records of EPICA Dome C and Dronning Maud Land ice cores
802 (East Antarctica), Quaternary Sci Rev, 29(1-2, SI), 146–159, doi:10.1016/j.quascirev.2009.10.009,
803 2010.

804 Stuiver, M. and Grootes, P. M.: GISP2 oxygen isotope ratios, Quaternary Res, 53(3), 277–283,
805 doi:10.1006/qres.2000.2127, 2000.

806 Stuiver, M., Grootes, P. M. and Braziunas, T. F.: The GISP2 delta O-18 climate record of the past
807 16,500 years and the role of the sun, ocean, and volcanoes, Quaternary Res, 44(3), 341–354,
808 doi:10.1006/qres.1995.1079, 1995.

809 van der Wel, L. G.: Analyses of water isotope diffusion in firn. Ph.D. Thesis, university of
810 Groningen, 2 March. 2012. Available through http://irs.ub.rug.nl/ppn/34029308X (last access: 10
811 February 2015), 2012.

812 van der Wel, L. G., Gkinis, V., Pohjola, V. A. and Meijer, H. A. J.: Snow isotope diffusion rates
813 measured in a laboratory experiment, J Glaciol, 57(201), 30–38, 2011a.

814 van der Wel, L. G., Streurman, H. J., Isaksson, E., Helsen, M. M., Van de Wal, R. S. W., Martma,
815 T. A., Pohjola, V. A., Moore, J. C. and Meijer, H. A. J.: Using high-resolution tritium profiles to
816 quantify the effects of melt on two Spitsbergen ice cores, J Glaciol, 57(206), 1087–1097, 2011b.

817 Vinther, B. M., Clausen, H. B., Johnsen, S. J., Rasmussen, S. O., Andersen, K. K., Buchardt, S. L.,
818 Dahl-Jensen, D., Seierstad, I. K., Siggaard-Andersen, M. L., Steffensen, J. P., Svensson, A., Olsen,
819 J. and Heinemeier, J.: A synchronized dating of three Greenland ice cores throughout the Holocene,
820 J Geophys Res-Atmos, 111, D13102, doi:10.1029/2005JD006921, 2006.

821 Vinther, B. M., Jones, P. D., Briffa, K. R., Clausen, H. B., Andersen, K. K., Dahl-Jensen, D. and
822 Johnsen, S. J.: Climatic signals in multiple highly resolved stable isotope records from Greenland,
823 Quaternary Sci Rev, 29(3-4), 522–538, doi:10.1016/j.quascirev.2009.11.002, 2010.

824 Weissberg, H. L.: Effective Diffusion Coefficient in Porous Media, J Appl Phys, 34(9), 2636–2639,
825 doi:10.1063/1.1729783, 1963.

826 Whillans, I. M. and Grootes, P. M.: Isotopic Diffusion in Cold Snow and Firn, J Geophys Res-
827 Atmos, 90(ND2), 3910–3918, doi:10.1029/JD090iD02p03910, 1985.

828 White, J. M. W., Barlow, L. K., Fisher, D., Grootes, P., Jouzel, J., Johnsen, S. J., Stuiver, M. and
829 Clausen, H.: The climate signal in the stable isotopes of snow from Summit, Greenland: Results of
830 comparisons with modern climate observations, J Geophys Res-Oceans, 102(C12), 26425–26439,
831 doi:10.1029/97JC00162, 1997.

832

833

834
835 **Table 1** The results for the diffusion length σ and for the net peak height for all profiles. The
836 increase of σ as a function of time is clearly visible. The uncertainties in the second column are
837 those from the fitting procedure. The final combined uncertainties in the results are presented in the
838 third column. Except for 2008, all measured values per year agree within their uncertainties. The net
839 peak height is also dependent on the initial thickness of the enriched layer. Therefore the found
840 peak height is variable within and between years.
841

profile	σ (cm)	uncertainty (cm)	δ^2H peak height (‰)
2008B	2.65 ± 0.03	0.25	678 ± 10
2008C	2.18 ± 0.13	0.15	99 ± 5
2009A	2.94 ± 0.03	0.10	258.9 ± 2.4
2009B	3.09 ± 0.10	0.25	91.9 ± 2.8
2010A	3.88 ± 0.03	0.15	391 ± 3
2010B	3.50 ± 0.07	0.25	83.6 ± 1.5
2010C	3.37 ± 0.16	0.3	59.3 ± 2.8
2011A	3.69 ± 0.05	0.25	254 ± 3
2011B	3.72 ± 0.08	0.15	102.9 ± 1.8

842
843
844
845 Figure captions
846
847 Figure 1 The production of the ^{2}H-labeled layer of snow at Summit, August 8, 2007. From left to
848 right the air compressor/water pump rack, the inflatable water container and the snow gun.
849
850
851 Figure 2 The depth of the enriched snow layer as a function of time, based on measuring the height
852 of each of the 5 poles that mark the field (lines), together with the points indicating the actual depth
853 of the enriched layer as revealed by the isotope measurements later in the lab (two to three points
854 per year).
855
856 Figure 3 Density measurements, with depth resolution of 10 cm, performed at our site in the years
857 2007, 2010 and 2011. The depths have been shifted such that our enriched layer (with an estimated
858 thicknes of typically 2 cm) is at relative depth zero. Our enriched layer, deposited in the end of the
859 summer of 2007, is on top of a summer layer with lower density than the preceding and following
860 winter layers.
861
862 Figure 4 The temperature registration of the thermocouple, at the same depth as the layer. The
863 dashed lines are interpolations for the times we did not have temperature measurements available.
864 The insert shows the first month of data in detail.
865
866 Figure 5 Two examples of δ^2H profiles obtained in this work, from 2008 (core B), and from 2011
867 (core A), respectively. The effect of diffusion is directly visible, both in the width of the peak, and
868 in its height. The δ^{18}O signal is shown in blue, with scale ratio 1:8 with respect to the δ^2H scale.
869

Figure 6 The nine net δ^2H profiles for the four consecutive years, together with the Gaussian fits. The width of the fit, which is the diffusion length σ, is listed in the plots. The brown circles are measurements discarded from the fit for various reasons (see text). The increase of σ over the years is clearly visible.

Figure 7 The results for the diffusion length σ. The points are the experimental results. The set of four higher-lying curves (one black, three in shades of blue) are the results of the numerical simulation using the Johnsen et al. (2000) model. The black one is the direct calculation of σ, the three blue ones result from the full numerical procedure starting with an enriched layer with 6, 18 and 30 mm initial thickness, respectively. Clearly, there is a systematic mismatch between the experimental results and the numerical simulations, increasing with time. The fit curve through the measurements is constructed by lowering the diffusivity by 25% in the first year, up to 40% in the last. Finally, the black dotted line shows the numerical result using a fixed, higher value for τ (1.6).

Figure 8 The actual peak height fits of the profiles (red circles). They are compared to the numerical simulations with initial layer thicknesses of 6, 18 and 30 mm, for which the diffusion length is fitted to the experimental points in figure 7. All experimental points are in the range spanned by the numerical calculations. The values for the ice layers that we removed from our profiles are also indicated (half-filled squares): all but one lie outside the possible range for diffused firn profiles, identifying them once more as ice layers.

Figure 9 Results of various tortuosity measurements from literature, with τ defined according to our equation (13). The symbols are the results of the various measurements: the red squares are laboratory firn diffusion measurements (by Jean-Baptiste et al., 1998 and van der Wel et al., 2011), the blue circles CO_2 and O_2 gas diffusion measurements through firn from Siple dome, Antarctica (Schwander et al., 1988), the green triangles SF_6 gas diffusion measurements through firn from Summit (Adolph and Albert, 2013; 2014). Finally pale brown triangles are the results by Fabre et al., (2000) for SF_6 gas diffusion in Vostok and Col du Dome. The black dash-dotted line is the parameterization for the Schwander et al. (1988) data in the Johnsen et al. (2000) model. The grey dashed curve is the tortuosity that is equivalent to the fit that Cuffey and Steig (1998) made to isotope seasonal cycles in the Summit firn layer. Furthermore, as a lower limit, we have included the theoretical result, interpreted as τ, by Weissberg (1963), which he derived for spheres that can partly overlap or even fuse. For discussion of the results, see text.

Table 1 The results for the diffusion length σ and for the net peak height for all profiles. The increase of σ as a function of time is clearly visible. The uncertainties in the second column are those from the fitting procedure. The final combined uncertainties in the results are presented in the third column. Except for 2008, all measured values per year agree within their uncertainties. The net peak height is also dependent on the initial thickness of the enriched layer. Therefore the found peak height is variable within and between years.

profile	σ (cm)	uncertainty (cm)	δ^2H peak height (‰)
2008B	2.65 ± 0.03	0.25	678 ± 10
2008C	2.18 ± 0.13	0.15	99 ± 5
2009A	2.94 ± 0.03	0.10	258.9 ± 2.4
2009B	3.09 ± 0.10	0.25	91.9 ± 2.8
2010A	3.88 ± 0.03	0.15	391 ± 3
2010B	3.50 ± 0.07	0.25	83.6 ± 1.5
2010C	3.37 ± 0.16	0.3	59.3 ± 2.8
2011A	3.69 ± 0.05	0.25	254 ± 3
2011B	3.72 ± 0.08	0.15	102.9 ± 1.8

9 Figure captions

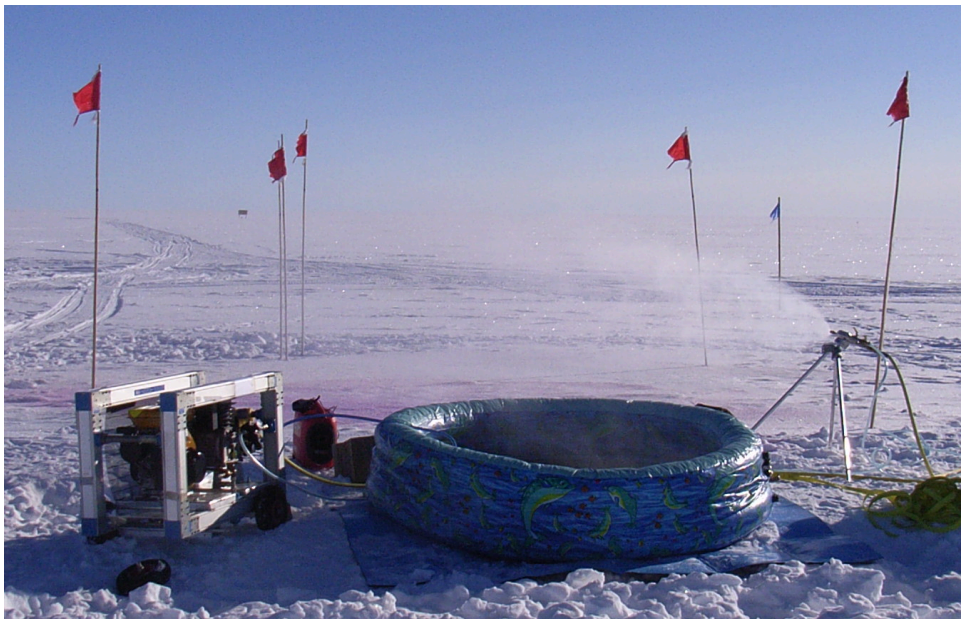

10

11 Figure 1 The production of the ^{2}H-labeled layer of snow at Summit, August 8, 2007. From left to
12 right the air compressor/water pump rack, the inflatable water container and the snow gun.
13

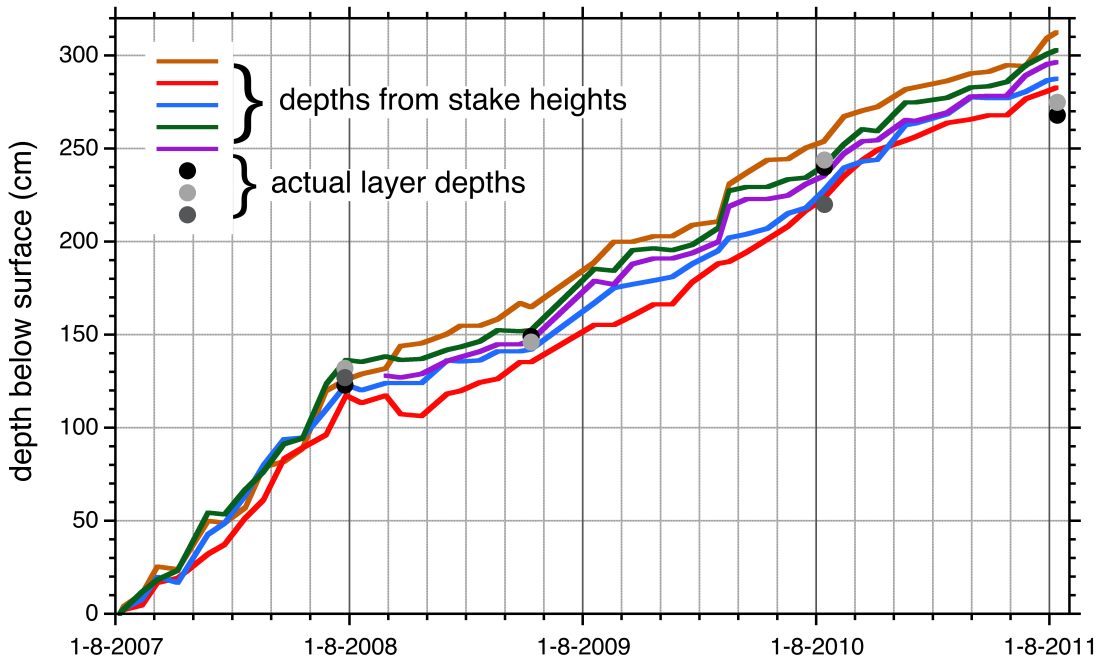

14

15 Figure 2 The depth of the enriched snow layer as a function of time, based on measuring the height
16 of each of the 5 poles that mark the field (lines), together with the points indicating the actual depth
17 of the enriched layer as revealed by the isotope measurements later in the lab (two to three points
18 per year).
19

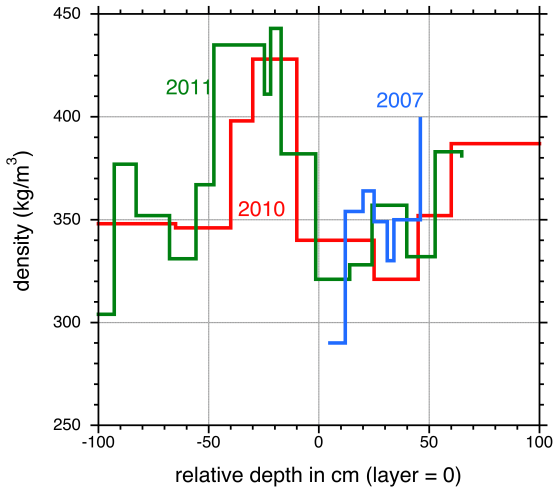

Figure 3 Density measurements, with depth resolution of 10 cm, performed at our site in the years 2007, 2010 and 2011. The depths have been shifted such that our enriched layer (with an estimated thicknes of typically 2 cm) is at relative depth zero. Our enriched layer, deposited in the end of the summer of 2007, is on top of a summer layer with lower density than the preceding and following winter layers.

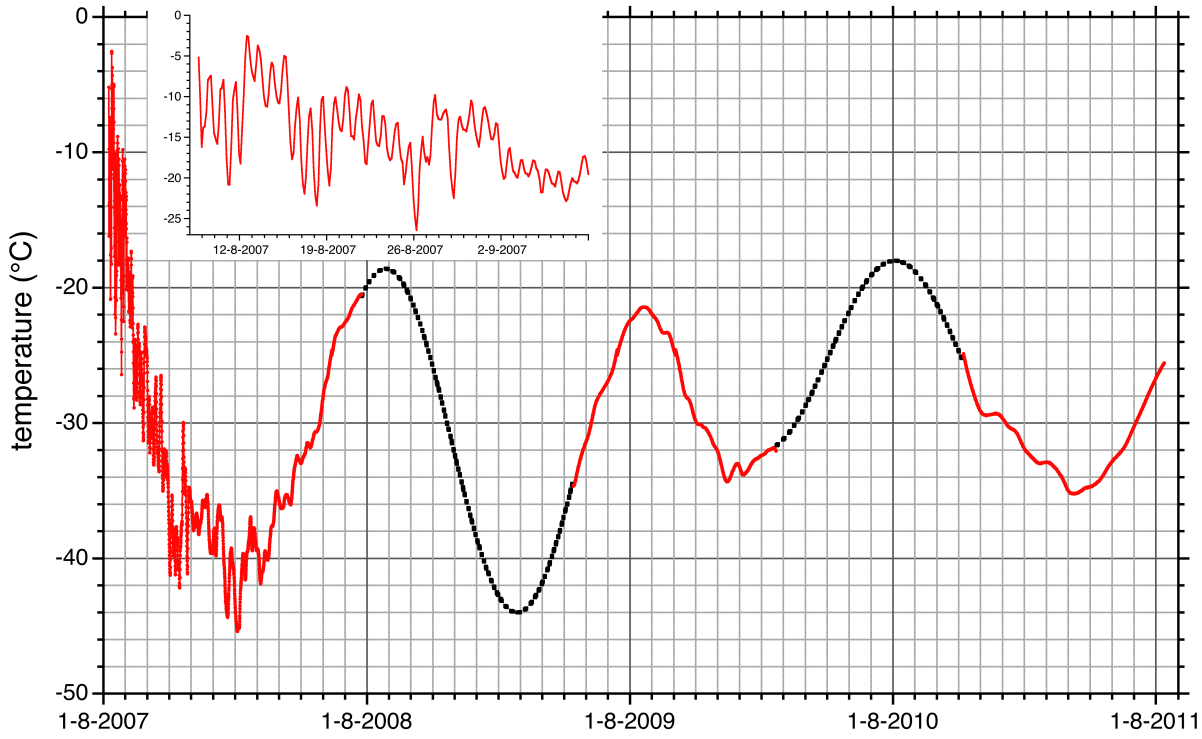

Figure 4 The temperature registration of the thermocouple, at the same depth as the layer. The dashed lines are interpolations for the times we did not have temperature measurements available. The insert shows the first month of data in detail.

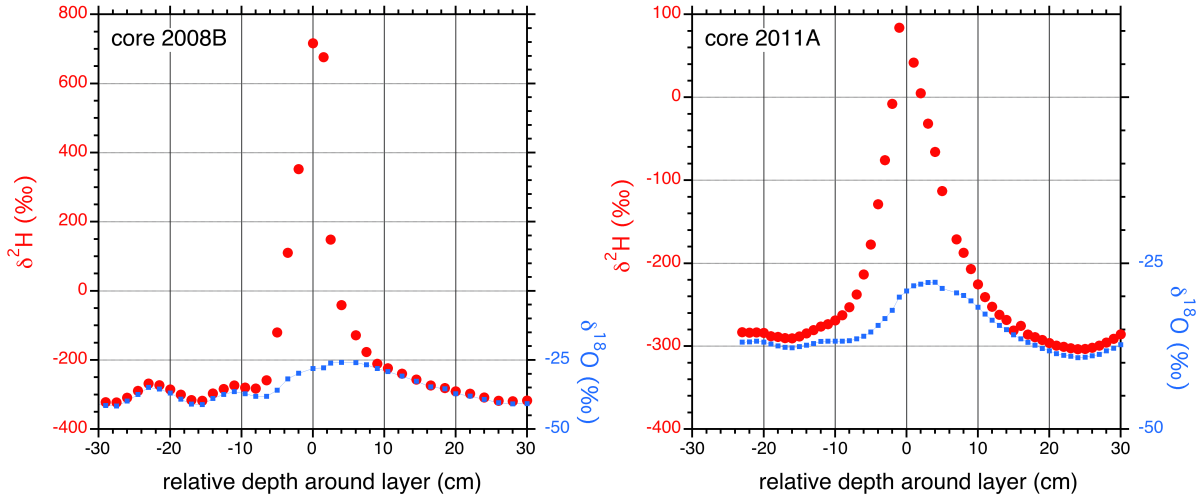

Figure 5 Two examples of δ^2H profiles obtained in this work, from 2008 (core B), and from 2011 (core A), respectively. The effect of diffusion is directly visible, both in the width of the peak, and in its height. The $\delta^{18}O$ signal is shown in blue, with scale ratio 1:8 with respect to the δ^2H scale.

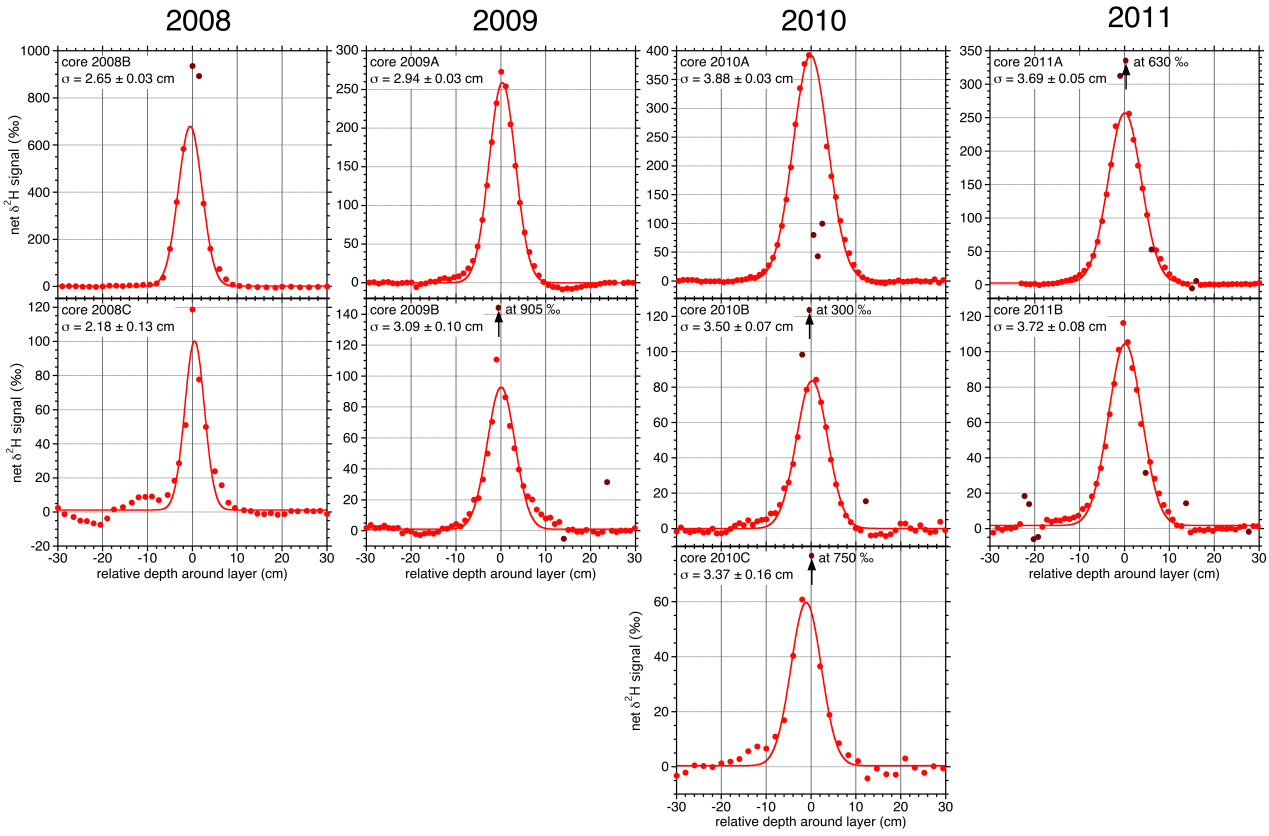

Figure 6 The nine net δ^2H profiles for the four consecutive years, together with the Gaussian fits. The width of the fit, which is the diffusion length σ, is listed in the plots. The brown circles are measurements discarded from the fit for various reasons (see text). The increase of σ over the years is clearly visible.

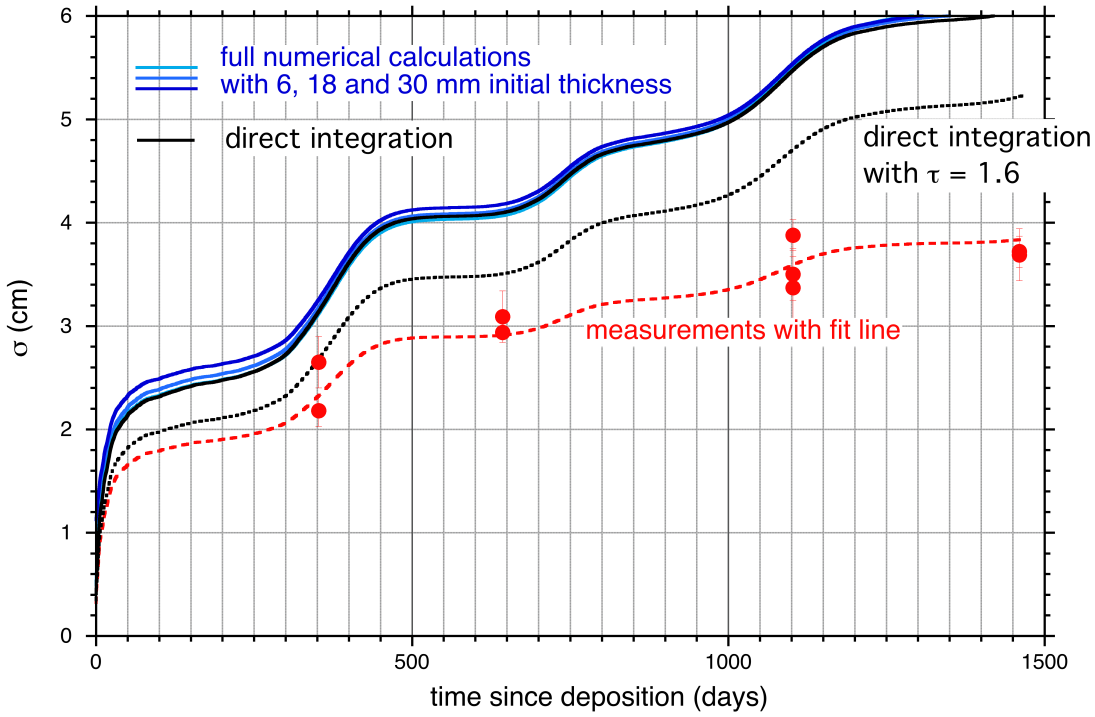

Figure 7 The results for the diffusion length σ. The points are the experimental results. The set of four higher-lying curves (one black, three in shades of blue) are the results of the numerical simulation using the Jo2000 model. The black one is the direct calculation of σ, the three blue ones result from the full numerical procedure starting with an enriched layer with 6, 18 and 30 mm initial thickness, respectively. Clearly, there is a systematic mismatch between the experimental results and the numerical simulations, increasing with time. The fit curve through the measurements is constructed by lowering the diffusivity by 25% in the first year, up to 40% in the last. Finally, the black dotted line shows the numerical result using a fixed, higher value for τ (1.6).

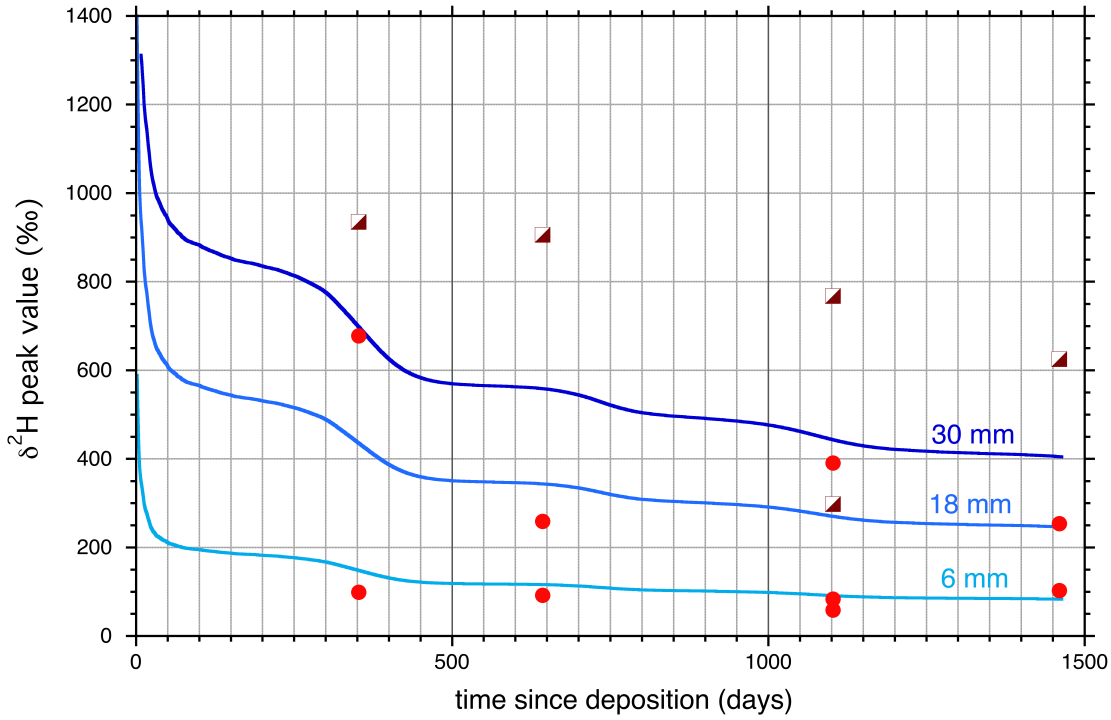

Figure 8 The actual peak height fits of the profiles (red circles). They are compared to the numerical simulations with initial layer thicknesses of 6, 18 and 30 mm, for which the diffusion length is fitted to the experimental points in figure 7. All experimental points are in the range spanned by the numerical calculations. The values for the ice layers that we removed from our profiles are also indicated (half-filled squares): all but one lie outside the possible range for diffused firn profiles, identifying them once more as ice layers.

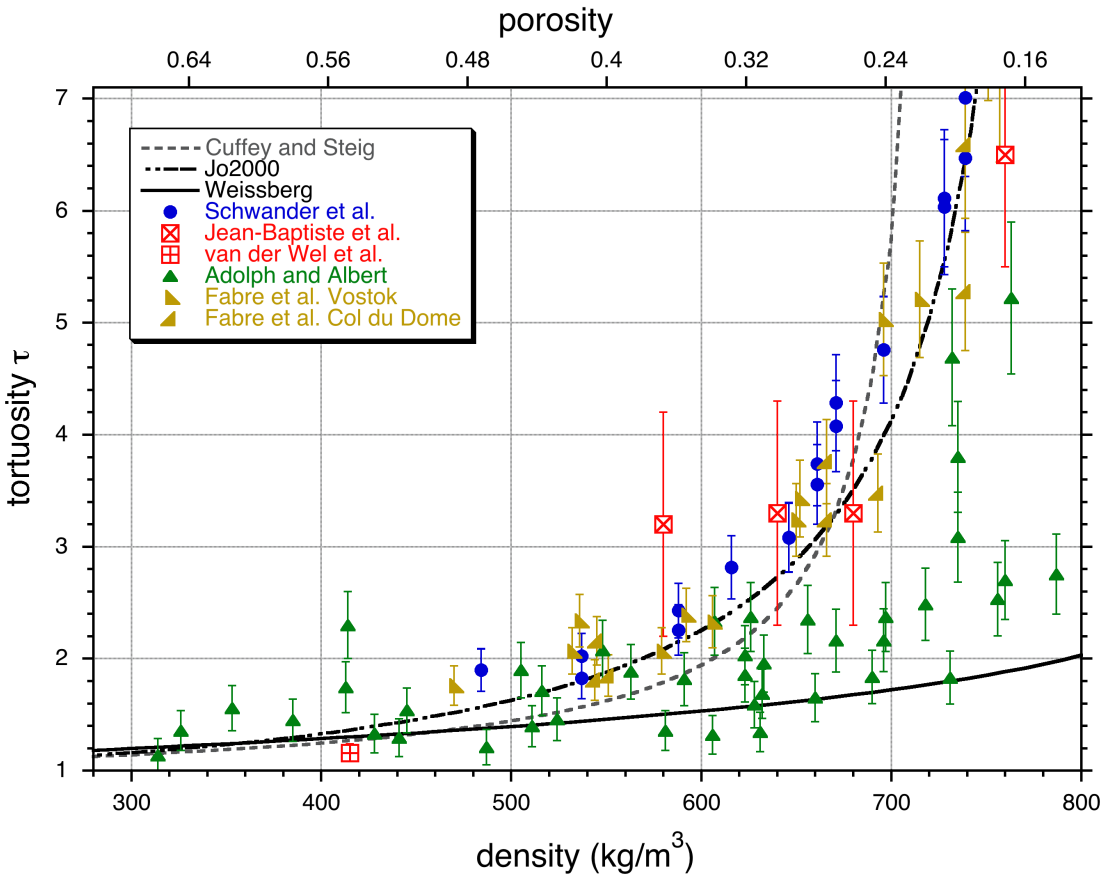

Figure 9 Results of various tortuosity measurements from literature, with τ defined according to our equation (13). The symbols are the results of the various measurements: the red squares are laboratory firn diffusion measurements (by Jean-Baptiste et al., 1998 and van der Wel et al., 2011), the blue circles CO_2 and O_2 gas diffusion measurements through firn from Siple dome, Antarctica (Schwander et al., 1988), the green triangles SF_6 gas diffusion measurements through firn from Summit (Adolph and Albert, 2013; 2014). Finally pale brown triangles are the results by Fabre et al., (2000) for SF_6 gas diffusion in Vostok and Col du Dome. The black dash-dotted line is the parameterization for the Schwander et al. (1988) data in the Jo2000 model. The grey dashed curve is the tortuosity that is equivalent to the fit that Cuffey and Steig (1998) made to isotope seasonal cycles in the Summit firn layer. Furthermore, as a lower limit, we have included the theoretical result, interpreted as τ, by Weissberg (1963), which he derived for spheres that can partly overlap or even fuse. For discussion of the results, see text.